Journal of Photochemistry and Photobiology A: Chemistry 217 (2011) 284–292

Contents lists available at ScienceDirect

Journal of Photochemistry and Photobiology A: Chemistry

journal homepage: www.elsevier.com/locate/jphotochem

Enhancement of the photodegradation of *N*-nitrosodimethylamine in water using amorphous and platinum manganese oxide catalysts

Homer C. Genuino [a], Eric C. Njagi [a], Evan M. Benbow [a], George E. Hoag [b], John B. Collins [b], Steven L. Suib [a,*]

[a] Department of Chemistry, University of Connecticut, 55 North Eagleville Rd., Unit 3060, Storrs, CT 06269, USA
[b] VeruTEK Technologies, Inc., 65 West Dudley Town Rd, Suite 100, Bloomfield, CT 06002, USA

ARTICLE INFO

Article history:
Received 27 July 2010
Received in revised form 12 October 2010
Accepted 21 October 2010
Available online 28 October 2010

Keywords:
NDMA
AMO
Pt/Mn_3O_4
Photodegradation
Hydroxyl and superoxide anion radicals

ABSTRACT

The enhancement of the photodegradation of toxic *N*-nitrosodimethylamine (NDMA) in water using amorphous manganese oxide (AMO) and platinum manganese oxide (Pt/Mn_3O_4) catalysts was investigated. Characterization of the catalysts was carried out using XRD, FESEM, TEM, EDXS, BET, XPS, and AOS. Pt/Mn_3O_4 and its precursor AMO, synthesized by a redox reaction of Mn^{2+} and Mn^{7+}, showed similar morphologies. High surface area AMO was confirmed to be amorphous, whereas Pt/Mn_3O_4 was a mixture of two crystalline structures. The optimum catalyst loading was 25 mg per 100 mL NDMA solution for which the photocatalytic activity was maximized. The average hydrodynamic particle size of a given amount of catalyst increased due to aggregation as a result of an increase in temperature during UV illumination ($\lambda = 254$ nm). Photocatalytic studies showed that NDMA degraded according to zero-order kinetics under air saturation at pH 7.0. AMO and Pt/Mn_3O_4 showed photostability and comparable activities with pure TiO_2 and platinized TiO_2. Mixed valencies of Mn and the presence of O_2 on the surface of the catalysts, which reacts with photogenerated electrons to form reactive oxygen species (hydroxyl and superoxide anion radicals), played significant roles in the enhancement of the photodegradation of NDMA in water.

1. Introduction

In recent years, *N*-nitrosodimethylamine (NDMA) has become a priority pollutant under the United States Environmental Protection Agency (US EPA) and has been classified by the World Health Organization as a potential carcinogen in humans [1–3]. NDMA can naturally be formed in the environment as a result of various chemical and biological processes involving precursor substances such as tertiary amines, dimethylamine (DMA), and natural organic matter [4,5]. Anthropogenic sources of NDMA such as release from agricultural, dye, cosmetic, food processing, polymer, rocket-fuel, and wastewater industries can largely contribute to the presence of NDMA in the environment [6–8]. The widespread presence of its precursors, resistance to biodegradation, high thermal stability, and excellent solubility in water make NDMA persistent and difficult to destroy once formed [5,8,9].

Removal of NDMA in the environment as a chemical contaminant [7] remains a challenge. The utilization of natural light to degrade NDMA is promising due to NDMA's weak UV absorption ($\lambda_{max} = 332$ nm) [10–12], but the rate of photolysis is slow and limited by the availability of sunlight in some areas. Treatment technologies such as direct UV photolysis, advanced oxidation/photooxidation, and reduction processes have been suggested to degrade NDMA in water. Direct UV photolysis is effective but is not economical on a large scale due to high intensity input requirements [11,12]. Advanced oxidation treatments using UV/pure and surface modified TiO_2, UV/O_3, and UV/H_2O_2 producing hydroxyl radicals (•OH) as primary oxidant may be limited by the amount of •OH they produce and the presence of •OH scavengers in water [13–15]. Further, addition of H_2O_2 does not significantly enhance the performance of medium-pressure UV lamps in NDMA degradation [16]. Recent studies on reductive destruction of NDMA in water include the use of bimetallic catalysts such as nickel–boron [17], nickel–iron [18], and palladium–indium [19]. However, these catalysts have not been extensively applied to groundwater and wastewater because of matrix effects associated with the complexity of these samples which could interfere in the determination of NDMA.

Manganese oxide catalysts are generally known as oxidants due to the presence of active oxygen species (in the lattice or adsorbed on the surface) [20] and are proven active for thermally and photochemically catalyzed reactions. This study describes the use of two Mn oxide catalysts, AMO and Pt/Mn_3O_4, to enhance the photodegradation of NDMA present in high concentrations in water at neutral pH. AMO catalysts prepared using $KMnO_4$ and oxalic acid as a reducing agent are known to demonstrate pho-

* Corresponding author. Tel.: +1 860 486 2797; fax: +1 860 486 2981.
E-mail address: Steven.Suib@uconn.edu (S.L. Suib).

1010-6030/$ – see front matter © 2010 Elsevier B.V. All rights reserved.
doi:10.1016/j.jphotochem.2010.10.021

tocatalytic activities for the oxidation of isopropanol to acetone with excellent selectivity at ambient temperature [21]. AMO has also been found to be an active photocatalyst in the oxidation of methyl bromide, methyl chloride, and methyl iodide [22] and in the decomposition of dimethyl methylphosphonate [23]. AMO may as well be applicable for the photodegradation of an organic pollutant such as NDMA. Noble metals such as Au, Ag, Pd, and Pt are known to enhance the photocatalytic efficiency of TiO_2 in degrading pollutants in water by retarding recombination of photogenerated electrons and holes [24]. A number of studies were conducted using pure and platinized TiO_2 (Pt/TiO_2) for UV degradation of pollutants including NDMA [13,25]. Investigating the catalytic activity of a platinum-containing Mn oxide with different properties from AMO toward NDMA photodegradation is therefore interesting.

The preparation and characterization of AMO and Pt/Mn_3O_4 are described here. Results from spectroscopic, chromatographic, and voltammetric studies are interpreted to study the role of the catalysts and the reactive oxygen species ($^{\bullet}OH$ and $^{\bullet}O_2^-$) that form, and the kinetics of catalyzed photodegradation of NDMA. This seems to be the first time that Mn oxide catalysts have been used to enhance the photodegradation of NDMA in water. The high photocatalytic activity, recyclability, hydrophobicity, relatively low cost, and low toxicity are some of the advantages of Mn oxide catalysts for large-scale environmental applications.

2. Materials and methods

2.1. Preparation of the catalysts

AMO was synthesized *via* a redox sol–gel method by adding 50 mL of 1.2 M $KMnO_4$ dropwise to 50 mL of 2.55 M $Mn(C_2H_3O_2)_2{\cdot}4H_2O$. The solution was stirred for 24 h and the black precipitate formed was washed with 1000 mL ultrapure water, dried in a vacuum at ambient temperature, and ground into powder. The Pt/Mn_3O_4 was synthesized by dissolving 2 g of prepared AMO to a solution made by dissolving 20 g of powdered polyvinylpyrollidone in ultrapure water. K_2PtCl_4 of 0.6220 g was then added to the mixture. The resulting mixture was purged with Ar gas for 1 h and then bubbled with H_2 gas. The reaction vessel was sealed and kept in an oven at 50 °C for 12 h and then washed. Finally, the solid was calcined in air at 150 °C for 5 h.

2.2. Characterization of the catalysts

Structural characterization of the catalysts was carried out using powder X-ray diffraction (XRD). The XRD patterns of the catalysts were recorded on a Scintag 2000 PDS diffractometer using Cu-Kα radiation (1.5418 Å wavelength), a beam voltage of 45 kV and a current of 40 mA. The sample scans were done at 2 degree $2\theta\ min^{-1}$.

The morphology of the catalysts was studied using field emission scanning electron microscopy (FESEM) and transmission electron microscopy (TEM). FESEM images were obtained using a Zeiss DSM 982 Gemini microscope equipped with a Schottky emitter at a beam current of 1 μA and accelerating voltage of 10–20 kV. Sample suspensions were prepared in ethanol and applied as a monolayer on gold-coated Si wafers. TEM images and Selected Area Electron Diffraction (SAED) patterns of the catalysts were obtained using a JEOL 2010 FasTEM microscope at an accelerating voltage of 200 kV. Sample suspensions were prepared using 2-propanol and deposited on carbon-coated Cu grids.

The compositions of the catalysts were determined using an AMRAY/LICO Model 9800 SEM equipped with an energy dispersive X-ray spectroscopy (EDXS) analyzer at an accelerating voltage of 20 kV. A standardless EDXS ZAF quantification method was used to obtain the compositions of the catalysts as atomic % (average value at three random locations).

The specific surface areas of the catalysts were determined using the Brunauer–Emmett–Teller (BET) method by acquiring N_2 adsorption and desorption isotherms at 77 K using a Micromeritics ASAP 2010 instrument system. The catalysts were pretreated by degassing them at 120 °C under vacuum for 2 h prior to BET analysis.

A PerkinElmer Physical Electronics Model 5300 X-ray photoelectron spectrometer (XPS) equipped with a monochromator Al Kα X-ray power source (250 W) with a pass energy of 50 eV and hemispherical analyzer was used to study the binding energies (BE) of Mn in the catalysts. The signal from adventitious carbon with BE of 284.6 eV was used as a reference.

The determination of average oxidation state (AOS) of Mn in the catalysts was carried out by potentiometric titrations [26]. First, the total Mn content was determined by digesting the sample with $HCl_{(aq)}$ to form Mn^{2+} in solution. To determine the concentration of Mn, the $Mn^{2+}{}_{(aq)}$ was then titrated with standard $MnO_4{}^-{}_{(aq)}$ containing $Na_4P_2O_7{\cdot}10H_2O_{(aq)}$ forming $Mn(H_2P_2O_7)^{3-}{}_{(aq)}$. The total MnO_2 content of the sample was also determined by reacting the sample with excess $Fe[NH_4]_2(SO_4)_{2(aq)}$ under N_2 atmosphere followed by back-titration of the excess $Fe^{2+}{}_{(aq)}$ with standard $MnO_4{}^-{}_{(aq)}$. The number of moles of oxygen in the form of MnO was obtained by the difference in the number of moles of Mn^{2+} and of MnO_2. On the basis of the total amount of charge due to oxygen in the compound, the AOS was then calculated.

2.3. Sample preparation and photocatalytic studies

In a typical experiment, 25 mg of the catalyst was added to a beaker containing 100 mL of 100 or 1000 μM NDMA solution. High concentrations of NDMA were used not only to allow better quantification but also to explore the applicability of this study in highly contaminated water. The heterogeneous mixture was then stirred for 30 min to attain equilibrium and sonicated for 15 min to uniformly disperse the catalyst particles prior to UV illumination. All mixtures were prepared using ultrapure water buffered with 4 mM bicarbonate and adjusted to pH 7.0 ± 0.1 by acid dilution using H_2SO_4. The pH of the mixture was measured using an Accumet pH meter 25.

Sixteen 15-W UV-C lamps emitting mainly monochromatic light with 99% emission at λ = 254 nm installed on the *Rayonet*® photochemical reactor were used as the constant UV source. The prepared mixture was transferred to a quartz cylindrical vessel with dimensions of 4.5 cm i.d. × 24 cm length and positioned at the center of the photoreactor (~10 cm away from the lamps). The mixture was then purged either with compressed air or Ar gas (ultra-high purity grades) for 30 min through an inlet port through a removable top. The UV lamps were stabilized for 5 min prior to illumination. The fan controlled the temperature inside the photoreactor fairly constant. UV illumination times were at 60 min intervals from 0 to 240 min performed with continuous stirring of the mixture. NDMA was extracted using continuous liquid–liquid extraction prior to gas chromatographic analysis as described in US EPA Method 3520C [27]. In another run, a desired volume (~10 mL) for spectroscopic analysis was withdrawn through a rubber septum using a glass syringe at various time intervals. Suspended catalysts were easily recovered from the mixture by centrifugation of the mixture for 30 min at 8000 rpm, subsequently washed and filtered through a Millipore filter (pore size 0.45 μm), and dried under vacuum at ambient temperature. Reacted catalysts were reused twice and characterized using XRD and AOS.

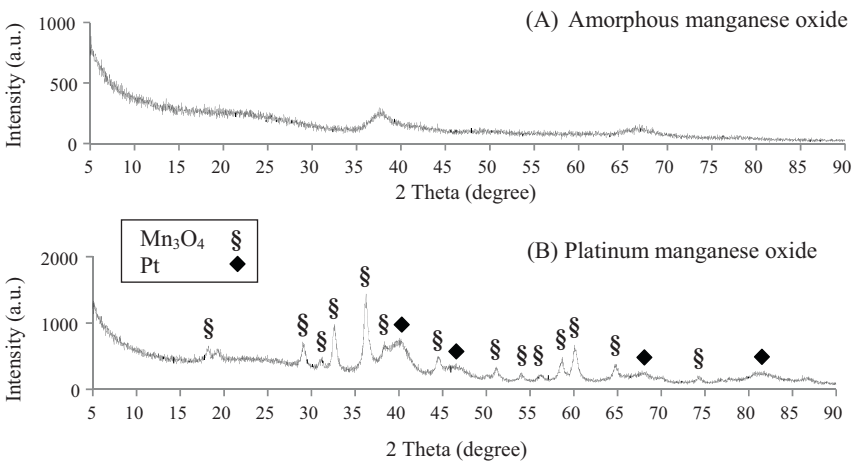

Fig. 1. Powder XRD patterns of sample (A) amorphous manganese oxide (AMO) and (B) platinum manganese oxide (Pt/Mn_3O_4) before photocatalytic reaction.

2.4. Analyses of reaction species and products

The analyses of reaction intermediates and products were carried out at pH 7.0 and ambient temperature. The concentrations of dissolved O_2 and temperatures of the mixture during UV illumination were measured using a YSI 550A DO instrument meter. Dynamic light scattering (DLS) experiments were performed using a Zetasizer Nano ZS90 equipped with 4 mW He–Ne ion laser (λ = 633 nm) at a measurement angle of 90°. This was utilized to determine the *Z*-average particle size of AMO suspended in NDMA solution. The V530 Jasco UV-Vis double-beam spectrophotometer equipped with silicon photodiode detector was used in the analysis of 1000 μM NDMA, NO_3^- and NO_2^- by a modified Nessler's method [28]. Dimethylamine and formaldehyde were analyzed using Umbreit [29] and Hantzsch [30] reactions, respectively. Ferrioxalate actinometry was performed for the determination of quantum yields for NDMA photolysis by obtaining absorbances of Fe(II)-1,10-phenanthroline solutions at 510 nm [31]. The UV–Vis spectrophotometer was also used in the generation of absorption spectra of solutions containing 2.2 mM NDMA and 0.24 mM tetranitromethane (TNM) with and without the catalysts after UV illumination for the detection of superoxide anion radicals ($^{\bullet}O_2^-$). External standard calibration method was used to correlate measured absorbance to concentration. Hydroxyl radicals produced in

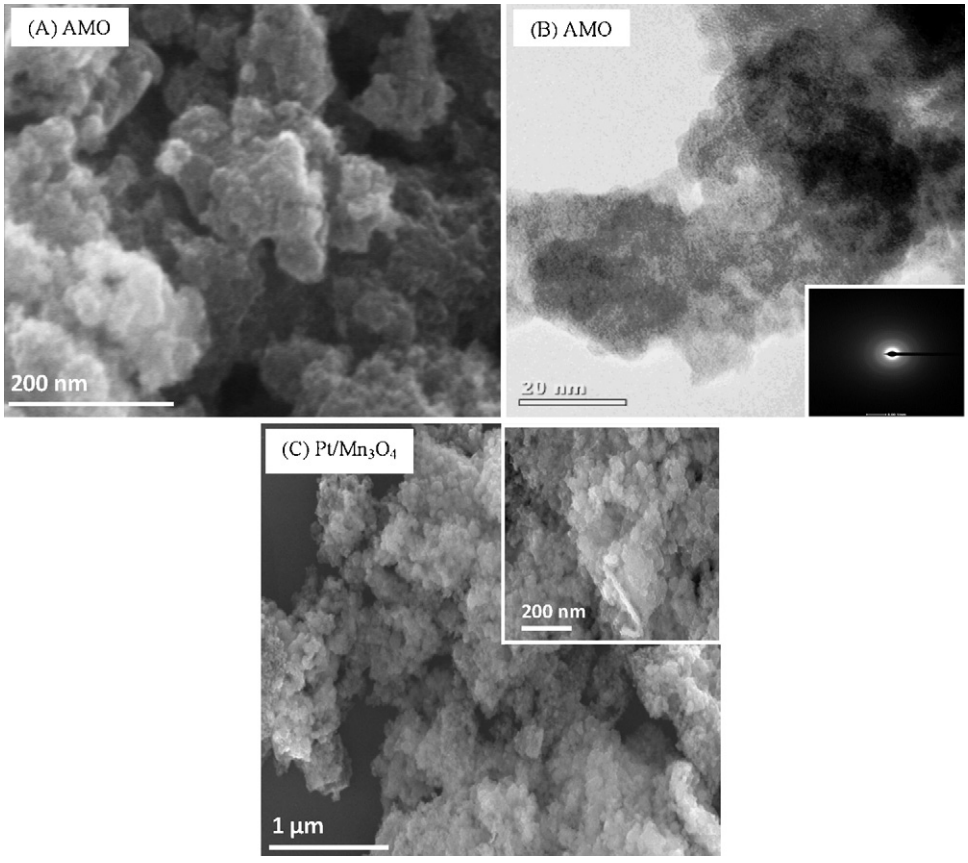

Fig. 2. FESEM images of sample (A) AMO and (C) Pt/Mn_3O_4. TEM image and SAED pattern (inset) of sample AMO (B). Inset in (C) shows magnified FESEM images of sample Pt/Mn_3O_4.

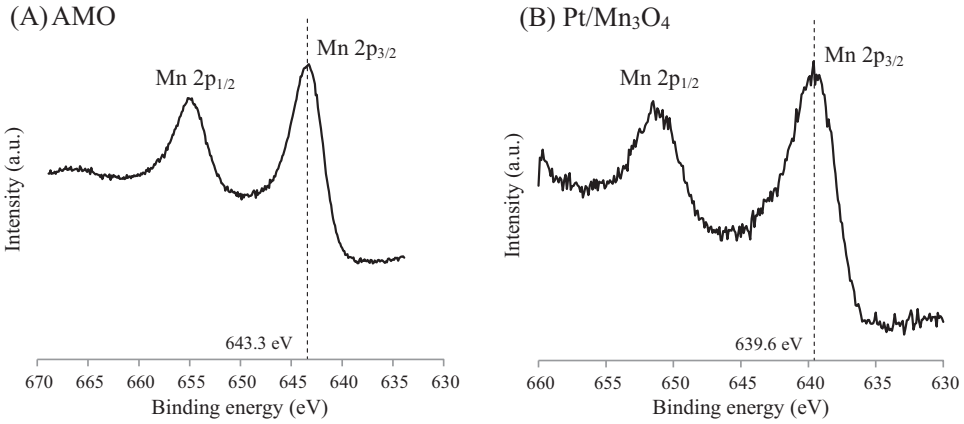

Fig. 3. Mn $2p_{3/2}$ XPS spectra of sample (A) AMO and (B) Pt/Mn_3O_4 before photocatalytic reaction.

water containing the catalysts after UV illumination were detected using 0.10 mM terephthalic acid solution. The photoluminescence (PL) spectra were measured on a Cary Eclipse Fluorescence spectrophotometer using excitation light of 320 nm.

Gas chromatographic analysis was performed on a Hewlett-Packard Model 5890A Series II system equipped with a mass selective detector (Hewlett-Packard Model 5871 Series). The 0.18 mm (i.d.) × 20 m (length) × 0.18 μm (film size) Agilent DB-17MS analytical column on (50%-phenyl)-methylpolysiloxane support was used for separation. A 1 μL sample was fed into the column using a 10-μL microsyringe. Helium carrier gas was set at a flow rate of about 10 $cm^3\ min^{-1}$. The injection port temperature and oven temperature range were set at 200 °C and 30–270 °C (rate = 10 °C min^{-1}), respectively. The retention time for NDMA was about 5.3 min. Quantitative analyses based on peak areas were performed. The concentrations of the NDMA were calculated following linear least square methods.

Cyclic voltammetric (CV) techniques were optimized and utilized for the oxygen reduction experiments performed on a computer-controlled CV-50W BAS Model 100B electrochemical analyzer with and without UV light. A three-electrode cell consisted of a Mn oxide catalyst slurry as the working electrode, a Ag/AgCl as the reference electrode, and a Pt wire as the counter electrode. The catalyst slurry was prepared by mixing 10 mg carbon powder, 10 mg AMO or Pt/Mn_3O_4 (10 mg carbon powder as blank), and 5 drops of polytetraflouroethylene binder solution in 5.0 mL ultrapure water. The resulting mixture was sonicated for 5 min and 20 μL of this was applied on the pyrolytic graphite electrode and dried overnight. A 20 mL volume of 1.0 M KOH aqueous solution (electrolyte solution) was purged either with pure O_2 or N_2 gas *via* a Teflon tube for 15 min. A quartz beaker was used as a cell compartment for experiments performed under UV light for 10–15 min. The scan ranges and scan rates used were +0.2 to −1.0 V and 50 mV s^{-1}, respectively. For CV experiments in non-aqueous aprotic solvents, saturated calomel electrode (SCE) was used as the reference electrode. A 0.1 M solution of tetrabutylammonium perchlorate (TBAP) was used as electrolyte solution. This was prepared by dissolving the proper amount of TBAP in dimethylsulfoxide (DMSO) or in dimethylformamide (DMF). The scan ranges and scan rates used were +0.20 to −1.2 V or −1.5 V and 50 mV s^{-1}, respectively.

3. Results

3.1. Characterization of the catalysts

The XRD patterns of the catalysts before photocatalytic reaction are shown in Fig. 1. The presence of weak and broad peaks at about 38° and 67° in sample AMO shown in Fig. 1A confirmed that AMO is almost completely amorphous. This is in agreement with the SAED pattern of AMO (Fig. 2B inset) where no spot patterns were observed and with diffraction rings that look fuzzy around the direct beam. Compared to AMO, Pt/Mn_3O_4 has completely different XRD patterns which show sharp and very intense peaks suggesting well-formed crystalline materials. The XRD pattern of sample Pt/Mn_3O_4 shown in Fig. 1B reveals diffraction peaks corresponding to Pt (*syn*) (JCPDS No. 04-802) and Mn_3O_4 (Hausmannite) (JCPDS No. 16-0154), thus the formula Pt/Mn_3O_4.

Fig. 2A presents the FESEM image of AMO which shows a non-distinct morphology that is composed of small clusters that are homogeneous throughout the material and with diameters ranging from approximately 50 to 100 nm. To further investigate this structure, TEM has been employed. The TEM image of AMO in Fig. 2B shows that these clusters are made up of nanoparticles of 5–15 nm sizes. A similar morphology to that of AMO is observed in the FESEM image of Pt/Mn_3O_4 shown in Fig. 2C. However, Pt/Mn_3O_4 forms larger aggregated clusters of smaller numerous nanoparticles that are regular in shape and size due to calcination.

The Mn/K atomic % ratios of AMO and Pt/Mn_3O_4 are 8.1 and 17.1, respectively. The Mn/Pt atomic % ratio for Pt/Mn_3O_4 is 40.1. The results of EDXS analyses are precise and are in good agreement with the expected results.

Fig. 3 shows the Mn 2p spectra for sample AMO and Pt/Mn_3O_4 before photocatalysis. The photoelectron binding energies (BE) corresponding to the Mn $2p_{3/2}$ transitions in AMO and Pt/Mn_3O_4 are 643.3 eV and 639.6 eV, respectively. These results indicate mixed valency of Mn (Mn^{2+}, Mn^{3+}, and Mn^{4+}) in both catalysts. However, it is difficult to accurately determine the oxidation state of Mn only by the BE of Mn $2p_{3/2}$ since the BEs for Mn^{2+}, Mn^{3+}, and Mn^{4+} overlap in the Mn $2p_{3/2}$ region.

The AOS values of Mn in AMO and Pt/Mn_3O_4 before photocatalytic reaction are 3.65 and 3.87, respectively, suggesting that Mn exists in mixed oxidation states. AMO has a BET surface area of 312 $m^2\ g^{-1}$, significantly higher than that of Pt/Mn_3O_4 (97 $m^2\ g^{-1}$).

3.2. Direct UV illumination

NDMA showed strong ($\pi \rightarrow \pi^*$ transition) and weak ($n \rightarrow \pi^*$ transition) absorptions in the 210–250 nm and 300–360 nm wavelength regions, respectively. UV illumination of 1000 μM NDMA solution using 254 nm UV lamps during the first 180 min decreases NDMA concentration by 50%. However, the absorbance readings in the weak absorption band centered at 330 nm remain almost unchanged. The irradiance spectrum of natural sunlight (>∼300 nm) overlaps within NDMA's weak absorption range [10]

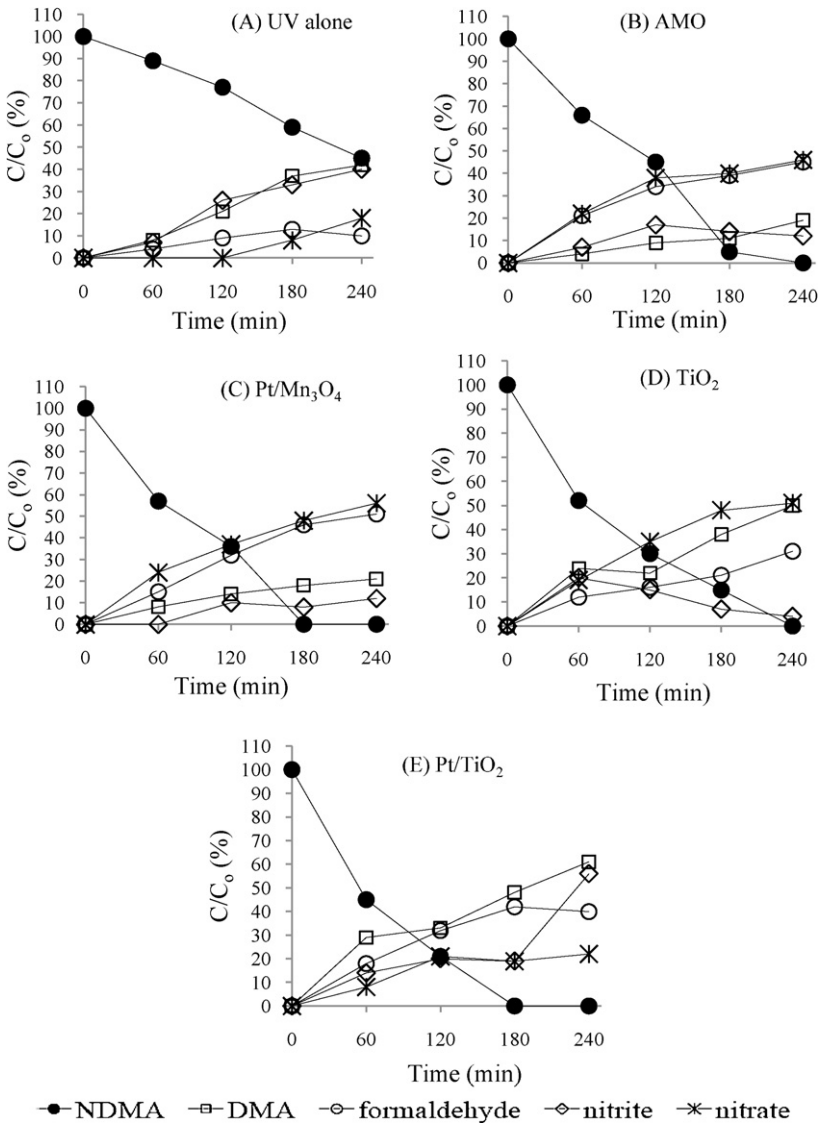

Fig. 4. Time course photodegradation of NDMA and formation of products (DMA, formaldehyde, NO_2^-, and NO_3^-) using (A) UV alone, and UV with (B) AMO, (C) Pt/Mn_3O_4, (D) TiO_2, and (E) Pt/TiO_2 catalysts under air-saturation at pH 7.0.

so a preliminary study using three UV-A/BL lamps ($\lambda = 350$ nm) was conducted. Results show that after 180 min of UV illumination, the concentration of NDMA in the weak absorption band decreased by almost 30%. The uncatalyzed UV illumination of 1000 μM NDMA targeting either strong or weak absorption bands follows first-order kinetics. A quantum yield of ~0.30 mol einstein^{-1} was determined for uncatalyzed NDMA photodegradation under air and Ar conditions at pH 7.0.

3.3. Effect of catalyst loading on NDMA photodegradation and the Z-average diameter of AMO

The optimum amount of AMO and Pt/Mn_3O_4 for NDMA photodegradation is 25 mg per 100 mL NDMA solution. DLS experiments were then performed to determine the *Z*-average diameter (intensity weighted average hydrodynamic size) of AMO particles suspended in NDMA aqueous solution at 25 and 100 mg catalyst loading. In general, the *Z*-average diameter of AMO particles in solution is at least 4× larger compared to its dehydrated particle size (TEM size). The *Z*-average diameters also increase with catalyst loading.

3.4. Enhanced NDMA photodegradation and product formation

The kinetic studies show that catalyzed and uncatalyzed photodegradation of 100 μM NDMA (Fig. 4A) obey zero-order kinetics consistent with the literature results [11]. The use of AMO (Fig. 4B) and Pt/Mn_3O_4 (Fig. 4C) in the presence of O_2 from air effectively enhances the photodegradation of NDMA as a function of time. Mixed-valent AMO and Pt/Mn_3O_4 have a significant difference in BET surface areas (215 $m^2\,g^{-1}$) and demonstrate photocatalytic activities. In the first 60 min, 34% of 100 μM NDMA are already degraded by AMO and 43% by Pt/Mn_3O_4, both with UV light. After 180 min, AMO and Pt/Mn_3O_4 achieve 95% and 100% NDMA photodegradation, respectively. Since both catalysts exhibit photoactivites, TiO_2 (Fig. 4D) and Pt/TiO_2 (Fig. 4E) were also tested for comparison purposes. Commercially available pure TiO_2 (Degussa P25) was used as received whereas Pt/TiO_2 was synthesized following the procedure in the literature [32]. Results reveal that Pt/TiO_2 is a better catalyst than pure TiO_2 and AMO but is comparable with Pt/Mn_3O_4 toward enhancing photodegradation of NDMA.

Dark experiments involving catalysts with and without O_2 showed no significant NDMA degradation. In the presence of UV light, however, AMO and Pt/Mn_3O_4 still showed better photocat-

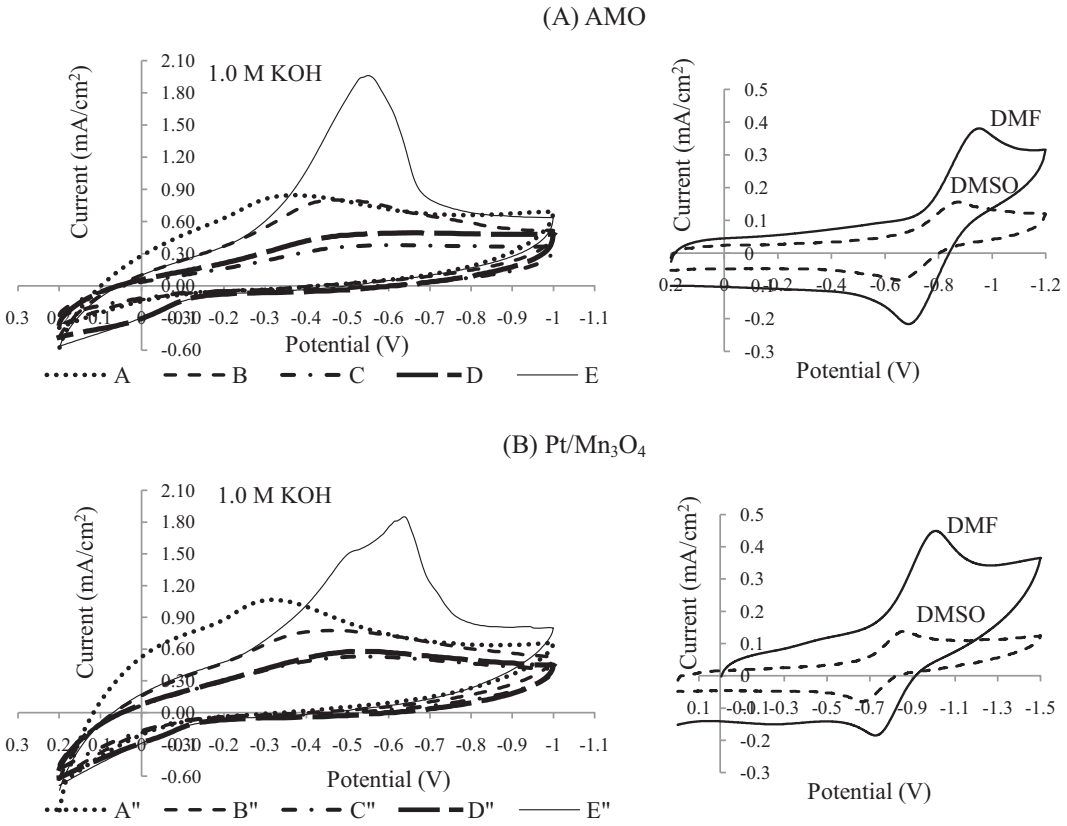

Fig. 5. Cyclic voltammograms of sample (A) AMO and (B) Pt/Mn_3O_4 in 1.0 M KOH and 0.1 M tetrabutylammonium perchlorate in DMSO and DMF solvents. (For CV studies in 1.0 M KOH: A curves: fresh catalysts, O_2-saturated; B curves: reused catalysts, O_2-saturated; C curves: reused catalysts, N_2-saturated; D curves: reused catalysts, N_2-saturated, UV light; E curves: reused catalysts, O_2-saturated, UV light.)

alytic activities than UV alone even in the absence of O_2 from air.

Formaldehyde and NO_3^- are the major oxidation photoproducts formed using AMO and Pt/Mn_3O_4. Dimethylamine and NO_2^- are also quantified. NO_2^- and NO_3^- form simultaneously and do not interfere with NDMA during UV photolysis. In the presence of AMO or Pt/Mn_3O_4, formation of NO_3^- is faster than NO_2^-. However, the concentration of NO_2^- is 2× higher than NO_3^- in the absence of the catalysts after 240 min UV light illumination. There was no significant difference in the average concentration of NDMA before and after the mixture was spiked with 50 and 100 μM of both NO_2^- and NO_3^- after 180 min of UV illumination.

3.5. O_2 generation, oxygen reduction studies, and detection of $^{\bullet}OH$ and $^{\bullet}O_2^-$ species

O_2 is generated in an Ar-saturated solution of NDMA in the presence of AMO or Pt/Mn_3O_4 catalyst and UV light. However, unlike in AMO, the concentration of dissolved O_2 using Pt/Mn_3O_4 gradually decreases upon further reaction for more than 120 min. Dark experiments and/or absence of the catalysts showed no detectable dissolved O_2.

Parallel studies by electrochemical reduction of O_2 using CV were conducted to further investigate the role of the catalysts, and thus of reactive oxygen species, in the photodegradation of NDMA. Fig. 5 shows that under O_2 saturation, both catalysts (fresh) (A curves) are electroactive in the potential window employed and have higher O_2 reduction peaks than the reused catalysts (B curves). The reduction peak potentials (∼−0.30 V) versus Ag/AgCl reference electrode for both catalysts in alkaline aqueous media are in the region corresponding to a 2-electron reduction step of O_2 to singly protonated peroxide ion, HO_2^- (Eq. (1)) [33]:

$$O_{2(g)} + H_2O_{(l)} + 2e^- \rightarrow HO_2^-{}_{(aq)} + OH^-{}_{(aq)} \quad (\text{noUVlight}) \qquad (1)$$

Minimal electroactivities are observed when the electrolyte solution was saturated with N_2 (C curves) for both catalysts. However, in the presence of UV light, small increase in the peak currents are observed (D curves). A much better electroactivity is restored when the electrolyte solution was repurged with O_2, indicating stability of the catalysts toward O_2 reduction. A significant increase in the reduction peak current and a shift toward more negative potential are observed for both catalysts when the solution was repurged with O_2 in the presence of UV light (E curves). Curves B and E for both catalysts fit perfectly from +0.20 V to −0.30 V suggesting that a different type of electron-transfer process, in addition to Eq. (1), occurs in the presence of UV light.

In O_2 saturated non-aqueous (aprotic) solutions, a 1-electron reduction of O_2 to O_2^- is observed using the same Mn oxide catalysts as working electrodes (Eq. (2)) [34]:

$$O_2 + e^- \leftrightarrow O_2^- \quad (\text{inaproticmedia, noUVlight}) \qquad (2)$$

The CV obtained using electrolyte solutions prepared using DMSO and DMF solvents, and TBAP for AMO and Pt/Mn_3O_4 are shown in Fig. 5, respectively, showing reduction (∼−0.86 V) and oxidation (∼−0.65 V) peak potentials versus SCE.

An indirect detection of $^{\bullet}OH$ and $^{\bullet}O_2^-$ species formed during UV illumination of water was performed using terephthalic acid and tetranitromethane (TNM) as chemical indicators, respectively. Fig. 6 presents the PL spectra of UV illuminated aqueous solutions of terephthalic acid in the presence of the catalysts. The visible emissions appear as strong and broad peaks with maxima at 427 nm, similarly observed for AMO and Pt/Mn_3O_4. The fluorescence inten-

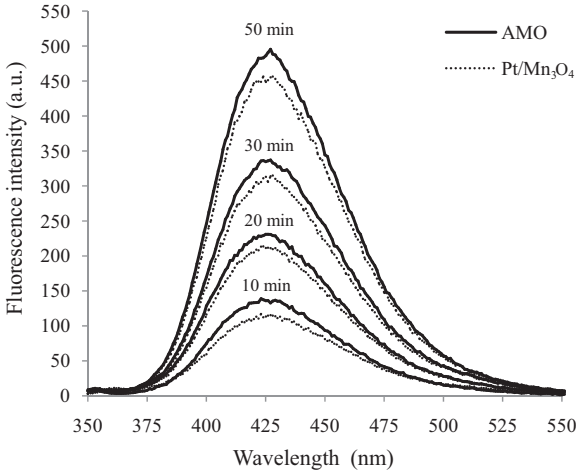

Fig. 6. Photoluminescence spectra of 0.10 mM terephthalic acid solution (adjusted to pH 7.0) with the catalysts using 320 nm excitation light. UV illumination (λ = 254 nm) times are 0, 10, 20, 30, and 50 min at pH 7.0 under air saturation. Excitation and emission slit widths are set at 5 nm.

sities are higher in the presence of the catalysts (higher in AMO than in Pt/Mn_3O_4) and increase with longer UV illumination times.

Fig. 7 shows the variations in the weak absorption band of NDMA solution centered at 330 nm (A) in the presence of TNM with and without the catalysts after UV illumination. In the presence of TNM and UV light for 10 min (optimum time) under Ar saturation, the NDMA peak shifts from 330 nm to 337 nm and increases absorbance by 30% (ΔA_{330} = 0.076) (B). However, broad and strong absorption bands centered at 345 nm are observed in the presence of TNM, UV light, and catalysts (C and D). Continuous UV illumination up to 30 min significantly decreases the absorption accompanied by a slight peak shift to a longer wavelength (350 nm) (E and F).

4. Discussion

In this study, absorption of incident photons by an optimum amount of suspended catalyst particles appears to enhance the photodegradation of NDMA. This was observed for both AMO and Pt/Mn_3O_4 even though AMO has much larger surface area (higher number of active sites) than Pt/Mn_3O_4. This suggests that there are other factors that govern the photocatalytic activities of AMO and Pt/Mn_3O_4 aside from surface area.

At constant NDMA concentration, excess loading of catalyst (>25 mg per 100 mL NDMA) generally brought about lower % NDMA photodegradation as observed for both AMO and Pt/Mn_3O_4. This could be due to hindered penetration of UV light by the excess catalyst particles with surfaces unbound to any NDMA molecules and thus do not take part in the reaction of NDMA, reactive oxygen

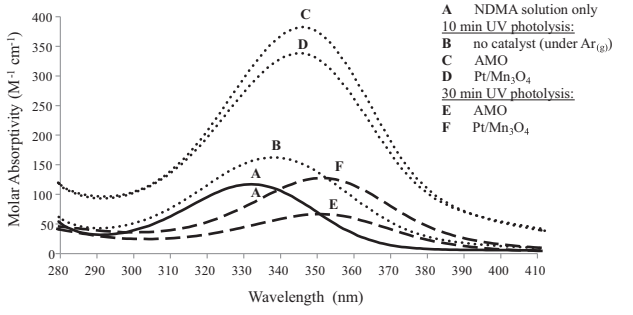

Fig. 7. UV–Vis absorption spectra of 2.2 mM NDMA aqueous solutions with 0.24 mM tetranitromethane indicator with and without the catalysts. UV illumination (λ = 254 nm) times are 0, 10, and 30 min at pH 7.0 under air saturation.

species, and photogenerated electrons and holes. Direct UV illumination of NDMA can also be blocked by excess catalysts through absorption. For DLS experiments, AMO was tested on the basis of its high surface area and small particle size compared to Pt/Mn_3O_4. Loadings of AMO greater than 25 mg could also reduce the availability of free space within which the catalyst particles can move in NDMA solution. This could be imparted by the tendency of the particles to aggregate in solution at a high loading (i.e. 100 mg per 100 mL) during the course of UV illumination as a result of an increase in temperature. Therefore, restricted diffusion due to AMO aggregation not only impacts mobility but could also explain why low percent NDMA degradation was observed for 100 mg AMO. The combined effect of solvation and the ability of AMO particles to aggregate with temperature as the catalyst loading is increased explain why the *Z*-average diameter of AMO is much larger than its TEM size. AMO (25 mg) is beneficial for the purpose of photodegrading thermally stable NDMA in water. Catalyst aggregation will affect particle transport and could be a crucial factor for catalyst recovery from suspension and recyclability especially when applied in aquatic environments or in ground and in wastewater.

Mixed valency is very common in Mn oxide materials and an important property in redox catalysis [35]. The AOS of Mn in AMO and Pt/Mn_3O_4 before reaction with NDMA under UV light suggests that the Mn in these samples exists in mixed oxidation states, most likely a mixture of Mn^{4+}, Mn^{3+}, and possibly Mn^{2+}, produced from the reduction of MnO_4^- (Mn^{7+}) during synthesis [22]. These results are in agreement with the Mn $2p_{3/2}$ XPS spectra of AMO and Pt/Mn_3O_4 (Fig. 3). Potassium ions counterbalance the charge as a result of the reduction of Mn^{4+}. The XRD pattern of Pt/Mn_3O_4 shows the existence of Pt and Mn_3O_4 (Hausmannite) crystal structures and also supports mixed valency of Mn in this material. The differences in the Mn^{3+} to Mn^{4+} ratio of AMO and Pt/Mn_3O_4 could enhance their photocatalytic activities since these Mn species have different electronic structures that have different effects on the band gaps of the Mn oxides. The significant increase in the AOS of Mn in AMO after reaction with NDMA (AOS_{after} = 3.90) suggests that there is a re-oxidation of Mn in the lower oxidation states (Mn^{2+} or Mn^{3+}) to Mn^{4+} by some regenerated O_2 species (Eq. (3)) during UV illumination. Although the amorphous structure of AMO did not change after reaction with NDMA and UV light, the significant change in the AOS of Mn due to re-oxidation of Mn in AMO is an important contributing factor as to its high activity in enhancing NDMA photodegradation. The XRD patterns of AMO and Pt/Mn_3O_4, and the AOS of Mn in Pt/Mn_3O_4 after photocatalytic reaction did not significantly change which suggest that UV illumination did not cause change in the original structures and therefore the same numbers of excited electrons and positive holes are possibly consumed during reaction and/or recombination. Further, the photocatalytic activities of AMO and Pt/Mn_3O_4 could be mainly due to the presence of surface adsorbed O_2.

When the reaction is carried out in an environment devoid of O_2, O_2 is evolved from the catalysts themselves to the NDMA solution containing partially reduced Mn oxide catalyst upon absorption of UV light. Eq. (3) shows the suggested sequence of O_2 release from the catalyst [21]. Surface adsorbed O_2 can accept electrons from photogenerated electrons (and/or reduced Mn species) and become negatively charged, O_2^- (bulk). Upon further absorption of UV light, O_2^- (bulk) react with electrons to form active oxygen radicals (O^-). O^- species react with electrons to form bulk O^{2-}. Oxygen evolution may be then due to migration of O^{2-} (bulk) to the surface of the catalyst as O_2 (regenerated) [21]:

$$\underset{\text{(surface adsorbed)}}{O_2} + e^- \xrightarrow{h\nu} \underset{\text{(bulk)}}{O_2^-} \xrightarrow[e^-]{h\nu} 2O^- \xrightarrow[e^-\ \text{(bulk)}]{h\nu} O^{2-} \xrightarrow{h\nu} 2O^- \xrightarrow{h\nu} \underset{\text{(on surface, regenerated)}}{O_2} \quad (3)$$

Some regenerated O_2 could be transformed into reactive oxygen species as peroxides or as oxygen radicals ($^{\bullet}OH$ and $^{\bullet}O_2^-$) which

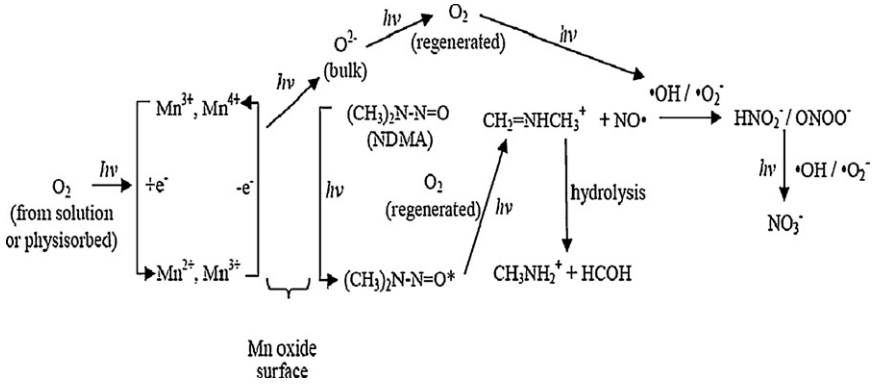

Fig. 8. Hypothetical mechanism for the photodegradation of NDMA forming NO_3^- and HCOH as major photoproducts using the Mn oxide catalysts [21,41].

due to instability may remain on the surface for a short period of time. Regenerated O_2 can be exhausted which leads to a slower rate of NDMA photodegradation or loss of activity. Spent catalysts can easily be rejuvenated in an O_2 environment which makes them reusable.

Significant electroactivity of AMO for O_2 reduction to HO_2^- could be associated with high concentrations of lattice defects and active sites of the amorphous material. Peroxide species can undergo decomposition to form hydroxide (Eq. (4)) [36] or superoxide species using metal oxides [37–39]. To explain the CV curves D and E in Fig. 4, the HO_2^- formed from Mn oxide-catalyzed electrochemical reduction of O_2 in protic solvent has likely undergone hydrolysis and decomposition into $^\bullet$OH and $^\bullet O_2^-$ through a disproportionation reaction in the presence of UV light. The $^\bullet$OH species were successfully detected and the visible emissions observed in the PL studies are attributed to the fluorescent product, monohydroxyterephthalate, formed by the reaction between terephthalic acid and photogenerated $^\bullet$OH (Fig. 6). As expected, the visible emission increases as $^\bullet$OH are produced with continued UV illumination. Considerably lower visible emission for Pt/Mn_3O_4 could be due to less structural defects in crystalline Pt/Mn_3O_4 than in AMO:

$$HO_2^-{}_{(aq)} + H_2O_{(l)} + 2e^- \rightarrow 3OH^-{}_{(aq)} \quad (4)$$

Previous study has shown that $^\bullet O_2^-$ are formed from UV illumination of alkaline electrolyte solution in the presence of O_2 [40]. In the present work, $^\bullet O_2^-$ are also formed in addition to $^\bullet$OH radicals. In the CV experiments using 1.0 M KOH, although $^\bullet O_2^-$ were not directly detected due to poor stability of superoxide species in aqueous solution, reactions in aprotic solvents provided clear evidence that superoxide anions are formed from reduction of O_2 using the catalysts. Ultimately, $^\bullet O_2^-$ were spectroscopically detected using TNM indicator. Eq. (5) shows the photoreduction of TNM, $C(NO_2)_4$, in the presence of $^\bullet O_2^-$ to form nitroform anion, $C(NO_2)_3^-$ [41]. $C(NO_2)_3^-$ in solution has a strong absorption band centered at 350 nm which explains the observed peak shifts and increase in UV absorbance of NDMA (Fig. 7). In the absence of any catalyst under Ar saturation, the slight peak shift and increase in the UV absorption could be explained by the direct UV illumination of NDMA and photoreduction of TNM to $C(NO_2)_3^-$ [41]. In the presence of the catalysts, the photoreduction of TNM is altered significantly (increase or decrease of ε) which could be due to regeneration of O_2 from the catalysts with continuous UV illumination:

$$C(NO_2)_{4(aq)} + {}^\bullet O_2^-{}_{(aq)} \rightarrow C(NO_2)_3^-{}_{(aq)} + NO_{2(g)} + O_{2(g)} \quad (5)$$

Previous studies showed that NO_2^- and NO_3^- produced as NDMA is photodegraded could possibly be competing with NDMA for absorption of UV light [11,42]. Here, interference studies suggest that almost all incident photons of $\lambda = 254$ nm are absorbed by the NDMA–catalyst mixtures due to low molar absorption coefficients of NO_2^- and NO_3^- compared with that of NDMA and presumably partly due to their dark colors imparted by the Mn oxide catalysts. A similar study supported this observation which showed that radical intermediates that were possibly generated from NO_2^- and NO_3^- during the complete UV illumination of NDMA at 254 nm did not interfere in its photodegradation [41].

The enhanced rate of NDMA photodegradation using AMO and Pt/Mn_3O_4 significantly produced HCOH and NO_3^- as the major oxidation photoproducts. A hypothetical mechanism for the enhancement of NDMA photodegradation using Mn oxide catalysts has therefore been proposed on the basis of experimental results and of previous studies suggesting photolytic pathways for the degradation of *N*-nitrosamines in water (Fig. 8) [41,43,44]. NDMA is adsorbed at the surface of the Mn oxide catalysts. Upon absorption of photons by the catalyst bound to NDMA, the electrons are excited from the valence band to their conduction bands leaving positive holes in the valence band. In Pt/Mn_3O_4, the electrons further transfer to Pt and the separation efficiency of the photoinduced electrons and holes is enhanced. The photogenerated electrons in the conduction band of Mn oxide react with dissolved O_2 in aerated NDMA solution to form reactive oxygen species such as $^\bullet$OH and $^\bullet O_2^-$. Under Ar saturation, the source of reactive oxygen species is UV illumination of regenerated O_2 (from physisorbed O_2) from the catalyst as depicted in Eq. (3). Initial absorption of UV light by NDMA also yields photoexcited NDMA [41,44]. The N-N bond in the photoexcited NDMA is photocleaved and in the presence of regenerated O_2, forms organic fragment as *N*-methylidenemethylamine ($CH_2{=}NHCH_3^+$) and NO fragment as $^\bullet$NO. Reactive oxygen species formed further oxidize $^\bullet$NO to produce a more stable product, NO_3^- and then desorbed from catalyst surface. *N*-methylidenemethylamine undergoes hydrolysis eventually forming formaldehyde and methylamine in 1:1 ratio.

5. Conclusion

Morphologically uniform and nanostructured amorphous manganese oxide (AMO) and crystalline Pt/Mn_3O_4 have been successfully synthesized and applied as catalysts for the enhancement of NDMA photodegradation with environmental relevance. Mixed valency of Mn in the catalysts was observed before photocatalytic reaction. AMO and Pt/Mn_3O_4 have provided significant improvements for the enhancement of photodegradation of NDMA in water in high concentrations. These catalysts can be good alternatives for established photocalysts such as TiO_2 and Pt/TiO_2 since they have comparable catalytic activities. AMO and Pt/Mn_3O_4 are stable toward O_2 reduction and UV light, and are reusable. Physisorbed O_2 reacts with photogenerated electrons to form reactive oxygen species and facilitates the trapping of photogenerated electrons and improves photocatalytic activity. This study provides

an important groundwork for future investigations of the enhancement of photodegradation of NDMA in water. Future studies should require experimental data from the application of these Mn oxide catalysts in the actual removal of NDMA from real and complex environmental samples.

Acknowledgments

The authors thank Heng Zhang for collecting the XPS data. This research was supported by VeruTEK Technologies and the U.S. Department of Energy, Office of Basic Energy Sciences, Division of Chemical, Biological and Geosciences.

Appendix A. Supplementary data

Supplementary data associated with this article can be found, in the online version, at doi:10.1016/j.jphotochem.2010.10.021.

References

[1] C.T. Gombar, H.M. Pylypiw Jr., G.W. Harrington, Cancer Res. 47 (1987) 343–347.
[2] E.C. Fleming, J.C. Pennington, R.A. Howe, M.R. Colsman, K.E. Garrett, B. Wachob, Hazard. Ind. Wastes 26 (1994) 285–292.
[3] *N*-nitrosodimethylamine in drinking-water, Background document for development of World Health Organization (WHO) Guidelines for Drinking-water Quality, Geneva, Switzerland, 2006.
[4] Z. Chen, R.L. Valentine, Environ. Sci. Technol. 40 (2006) 7290–7297.
[5] A.C. Gerecke, D.L. Sedlak, Environ. Sci. Technol. 37 (2003) 1331–1336.
[6] W.A. Mitch, D.L. Sedlak, Environ. Sci. Technol. 36 (2002) 588–595.
[7] W.A. Mitch, J.O. Sharp, R.R. Trussell, R.L. Valentine, L. Alvarez-Cohen, D.L. Sedlak, Environ. Eng. Sci. 20 (2003) 389–404.
[8] W.A. Mitch, D.L. Sedlak, Environ. Sci. Technol. 38 (2004) 1445–1454.
[9] I. Najm, R. Trussell, J. Am. Water Works Assoc. 93 (2001) 92–99.
[10] M.H. Plumlee, M. Reinhard, Environ. Sci. Technol. 41 (2007) 6170–6176.
[11] M.I. Stefan, J.R. Bolton, Helv. Chim. Acta 85 (2002) 1416–1426.
[12] Orange County Water District takes a proactive stance on newly regulated compound N-nitrosodimethylamine: OCWD recommends taking two drinking water wells out of service, Press Release from Orange County Water District, Fountain Valley, CA, USA, 2000.
[13] J. Lee, W. Choi, Environ. Sci. Technol. 39 (2005) 6800–6807.
[14] C. Lee, W. Choi, J. Yoon, Water Res. 41 (2005) 581–590.
[15] C. Lee, C. Schmidt, J. Yoon, U. von Gunten, Environ. Sci. Technol. 41 (2007) 2056–2063.
[16] C.M. Sharpless, K.G. Linden, Environ. Sci. Technol. 37 (2003) 1933–1940.
[17] A.J. Frierdich, C.E. Joseph, T.J. Strathmann, Appl. Catal. B: Environ. 90 (2009) 175–183.
[18] L. Gui, R.W. Gillham, R.W. Gillham, Environ. Sci. Technol. 34 (2000) 3489–3494.
[19] M.G. Davie, K. Shih, F.A. Pacheco, J.O. Leckie, M. Reinhard, Environ. Sci. Technol. 42 (2008) 3040–3046.
[20] S. Jana, S. Praharaj, S. Panigrahi, S. Basu, S. Pande, C.-H. Chang, T. Pal, Org. Lett. 9 (2007) 2191–2193.
[21] H. Cao, S.L. Suib, J. Am. Chem. Soc. 116 (1994) 5334–5342.
[22] J. Chen, J.C. Lin, V. Purohit, M.B. Cutlip, S.L. Suib, Catal. Today 33 (1997) 205–214.
[23] S.R. Segal, S.L. Suib, Chem. Mater. 11 (1999) 1687–1695.
[24] A. Mill, S. Le Hunte, J. Photochem. Photobiol. A: Chem. 108 (1997) 1–35.
[25] B. Kraeutler, A.J. Bard, J. Am. Chem. Soc. 100 (1978) 2239.
[26] D. Glover, B. Schumm Jr., A. Kozowa, Handbook of Manganese Dioxides Battery Grade, International Battery Materials Association, Cleveland, OH, USA, 1989.
[27] US EPA Method 3520C, Continuous Liquid–Liquid Extraction, Revision 3, 1996.
[28] G.T. Richardson, J.A. Davies, J.G. Edwards, Fresenius J. Anal. Chem. 343 (1992) 473–474.
[29] G.J. Hanna, in: S. Siggia (Ed.), Instrumental Methods of Organic Functional Group Analysis, Wiley-Interscience, New York, USA, 1972.
[30] T. Nash, J. Biochem. 55 (1953) 416.
[31] C.G. Hatchard, C.A. Parker, Proc. R. Soc. Lond. A 235 (1956) 518–536.
[32] J. Lee, H. Park, W. Choi, Environ. Sci. Technol. 36 (2002) 5462–5468.
[33] L. Mao, D. Zhang, T. Sotomura, K. Nakatsu, N. Koshiba, T. Ohsaka, Electrochim. Acta 48 (2003) 1015–1021.
[34] D.L. Maricle, W.G. Hodgson, Anal. Chem. 37 (1965) 1562–1565.
[35] F. Kapteijn, L. Singoredjo, A. Andreini, J.A. Moulijn, Appl. Catal. B: Environ. 3 (1994) 173–189.
[36] Holleman-Wiberg, The Chalcogen Group. Inorganic Chemistry, Academic Press, New York, 2001, pp. 473–475.
[37] Y. Ono, T. Matsumura, N. Kitajima, S.I. Fukuzumi, J. Phys. Chem. 81 (1977) 1307.
[38] N. Kitajima, S. Fukuzumi, Y. Ono, J. Phys. Chem. 82 (1978) 1505.
[39] S. Do, B. Batchelor, H. Lee, S. Kong, Chemosphere 75 (2009) 8–12.
[40] Y. Ilan, J. Rabani, A. Henglein, J. Phys. Chem. 80 (1976) 1558.
[41] C. Lee, W. Choi, J. Yoon, Environ. Sci. Technol. 39 (2005) 9702–9709.
[42] C. Lee, J. Yoon, J. Photochem. Photobiol. A: Chem. 189 (2007) 128–134.
[43] J. Polo, Y.L. Chow, J. Natl. Cancer Inst. 56 (1976) 997–1001.
[44] C. Lee, W. Choi, Y.G. Kim, J. Yoon, Environ. Sci. Technol. 39 (2005) 2101–2106.